Facultad de Ciencias
Universidad de Cantabria

Search for dark matter production in association with top quarks in the dilepton final state at $\sqrt{s} = 13$ TeV

A thesis submitted in fulfillment of the requirements for the

Degree of Doctor of Philosophy

Written by

Cédric Prieëls

Under the supervision of

Jónatan Piedra Gómez
Pablo Martínez Ruiz del Árbol

Santander, June 2020

Facultad de Ciencias
Universidad de Cantabria

Búsqueda de materia oscura en asociación con quarks top en el estado final dileptónico a $\sqrt{s} = 13$ TeV

Memoria para optar al

Grado de doctor

Escrita por

Cédric Prieëls

Bajo la supervisión de

Jónatan Piedra Gómez
Pablo Martínez Ruiz del Árbol

Santander, Junio 2020

Abstract

Resumen

Acknowledgments

Acronyms used

ADMX Axion Dark Matter Experiment

ALICE A Large Ion Collider Experiment

AMS Alpha Magnetic Spectrometer

AOD Analysis Object Data

ATLAS A Toroidal LHC ApparatuS

BDT Boosted Decision Trees

BR Branching Ratio

BSM Beyond the Standard Model

BW Breit-Wigner

CAST CERN Axion Solar Telescope

CERN European Council for Nuclear Research

CL Confidence Level

CMB Cosmic Microwave Background

CMS Compact Muon Solenoid

CSC Cathode Strip Chamber

CR Control Region

CSV Combined Secondary Vertex

CTA Cherenkov Telescope Array

DAQ Data Acquisition System

DAS Data Aggregation System

DCS Detector Control System

DQM Data Quality Monitoring

DM Dark Matter

DMWG Dark Matter Working Group

DNN Deep Neural Network

DT Drift tube

DY Drell-Yan

ECAL Electromagnetic Calorimeter

EDM Event Data Model

EFT Effective Field Theory

EWK Electroweak

FR Fake Rate

FSR Final State Radiation

GEM Gas Electron Multiplier

GSF Gaussian Sum Filter

HCAL Hadronic Calorimeter

HLT High-Level Trigger

HO Hadron Outer

IACT Imaging Atmospheric Cherenkov Telescopes

IAXO International AXion Observatory

ISR Initial State Radiation

KF Kalman Filter

L1 Level-1 Trigger

LAT Fermi Large Telescope

LEP Large Electron Positron collider

LHC Large Hadron Collider

LNGS Laboratori Nazionali del Gran Sasso

LO Leading Order

LS Long Shutdown

MACHO Massive Compact Halo Object

MC Monte Carlo

MET Missing Transverse Energy

MFV Minimal Flavour Violation

ML Machine Learning

MPI Multiple Parton Interaction

MSSM Minimal Supersymmetric Standard Model

MVA Multi-Variate Analysis

NFW Navarro-Frenk-White

NLO Next to Leading Order

PDF Parton Density Function

PF Particle Flow

POG Physics Object Group

PR Prompt Rate

PS Proton Synchrotron

PU Pile Up

PUPPI Pileup Per Particle Identification

PV Primary Vertex

QCD Quantum ChromoDynamics

QFT Quantum Field Theory

RMS Root Mean Square

RPC Resistive Plate Chamber

SC Super Cluster

SD Spin Dependent

SF Scale Factors

SI Spin Independent

SM Standard Model

SPS Super Proton Synchrotron

SR Signal Region

TEC Tracker EndCap

TIB/TBD Tracker Inner Barrel and Disks

TOB Tracker Outer Barrel

UE Underlying Event

UED Universal Extra Dimensions

VBF Vector Boson Fusion

WIMP Weakly Interactive Massive Particle

WP Working Point

Contents

1 Event selection **1**

1.1 Objects selection . . . 1

1.1.1 Triggers selection . . . 1

1.1.2 Electrons selection . . . 3

1.1.3 Muons selection . . . 6

1.1.4 Jet selection . . . 6

1.2 Signals regions . . . 6

1.3 Control regions . . . 8

1.3.1 Same sign control region . . . 8

1.4 Background-signal discrimination . . . 8

1.4.1 Discriminating variables . . . 8

1.4.2 Neural network . . . 10

2 Results and interpretations **11**

2.1 Systematics and uncertainties . . . 11

2.2 Results . . . 11

3 Conclusions **13**

3.1 Future prospects . . . 13

Appendices **15**

A Samples used **17**

A.1 Data samples . . . 17

A.2 Signal samples . . . 17

A.3 Backgrounds samples . . . 17

B Neural network optimization **21**

Bibliography **25**

Chapter 1

Event selection

This Chapter will be dedicated to the analysis itself, by defining first of all the different objects actually used in this case, along with the actual selection that has been applied to enhance the quality of such objects in this particular search in Section 1.1. Then, the different Signal Regions (SRs) defined in which a high purity of signal is expected are defined in Section 1.2 while all the different Control Regions (CRs) defined in order to check the behavior of the Monte Carlo (MC) simulation performed for the major backgrounds on this analysis, such as the single top or Standard Model (SM) $t\bar{t}$ production, will be introduced in Section 1.3.

Finally will come a description about the different variables expected to naturally introduce some discrimination of the $t/\bar{t}$ and $t\bar{t}$+DM signals with respect to the different backgrounds in Section 1.4, along with a global description of the Machine Learning (ML) techniques employed in order to optimize the discriminating power of these variables in the best way possible.

1.1 Objects selection

We already described what to expect from a typical $t/\bar{t}$ or $t\bar{t}$+DM signal: the typical signature of such signals is made out of a certain number of b tagged jets along with two leptons (electrons and/or muons) and some Missing Transverse Energy (MET) coming from the two Dark Matter (DM) particles created along the way. It is therefore extremely important to describe the Working Point (WP) chosen and the selection applied in order to select the objects of the analysis, such as the leptons and the jets used, in such a way to optimize the lepton reconstruction efficiency while reducing as much as possible the possible misidentification rates of such objects.

First of all, the different triggers used to collect the data will be detailed in Section 1.1.1. Then, the leptons used in this analysis will be introduced in Sections 1.1.2 (for electrons) and 1.1.3 (for muons). Finally, given the nature of the DM signal searched for, a complete description of the jets selected in the analysis will be necessary and performed in Section 1.1.4.

1.1.1 Triggers selection

The triggers, described in Section **??**, and particularly the trigger paths chosen are an important part of each analysis since they will describe the kind of data that can be collected and therefore analyzed. The triggers used in this analysis for the years 2016, 2017 and 2018 can be found in Tables 1.1, 1.2 and 1.1 respectively.

Dataset	Run range	**High-Level Trigger (HLT) trigger path**
SingleMu	[273158,284044]	HLT_IsoMu24_v*
		HLT_IsoTkMu24_v*
SingleEle	[273158,284044]	HLT_Ele27_WPTight_Gsf_v*
		HLT_Ele25_eta2p1_WPTight_Gsf_v*
DoubleEG	[273158,284044]	HLT_Ele23_Ele12_CaloIdL_TrackIdL_IsoVL_DZ_v*
DoubleMu	[273158,281612]	HLT_Mu17_TrkIsoVVL_Mu8_TrkIsoVVL_v*
		HLT_Mu17_TrkIsoVVL_TkMu8_TrkIsoVVL_v*
	[281613,284044]	HLT_Mu17_TrkIsoVVL_Mu8_TrkIsoVVL_DZ_v*
		HLT_Mu17_TrkIsoVVL_TkMu8_TrkIsoVVL_DZ_v*
MuonEG	[273158,278272]	HLT_Mu8_TrkIsoVVL_Ele23_CaloIdL_TrackIdL_IsoVL
		HLT_Mu23_TrkIsoVVL_Ele12_CaloIdL_TrackIdL_IsoVL
	[278273,284044]	HLT_Mu8_TrkIsoVVL_Ele23_CaloIdL_TrackIdL_IsoVL_DZ_v*
		HLT_Mu23_TrkIsoVVL_Ele12_CaloIdL_TrackIdL_IsoVL_DZ_v*

Table 1.1: 2016 trigger paths considered for this analysis.

Dataset	Run range	**HLT trigger path**
SingleMu	[297046,306462]	HLT_IsoMu27_v*
EGamma	[297046,306462]	HLT_Ele35_WPTight_Gsf_v*
		HLT_Ele23_Ele12_CaloIdL_TrackIdL_IsoVL_v*
DoubleMu	[297046,299329]	HLT_Mu17_TrkIsoVVL_Mu8_TrkIsoVVL_DZ_v*
	[299368,306462]	HLT_Mu17_TrkIsoVVL_Mu8_TrkIsoVVL_DZ_Mass8_v*
MuonEG	[297046,306462]	HLT_Mu12_TrkIsoVVL_Ele23_CaloIdL_TrackIdL_IsoVL_DZ_v*
	[297046,299329]	HLT_Mu23_TrkIsoVVL_Ele12_CaloIdL_TrackIdL_IsoVL_DZ_v*
	[299368,306462]	HLT_Mu23_TrkIsoVVL_Ele12_CaloIdL_TrackIdL_IsoVL_v*

Table 1.2: 2017 trigger paths considered for this analysis.

Dataset	Run range	**HLT trigger path**
SingleMu	[315252,325172]	HLT_IsoMu24_v*
		HLT_Mu5_v*
	[314859,325175]	HLT_IsoMu27_v*
EGamma	[315252,325172]	HLT_Ele32_WPTight_Gsf_v*
		HLT_Ele35_WPTight_Gsf_v*
		HLT_Ele23_Ele12_CaloIdL_TrackIdL_IsoVL_v*
DoubleMu	[315252,325172]	HLT_Mu17_TrkIsoVVL_Mu8_TrkIsoVVL_DZ_Mass3p8_v*
		HLT_Mu17_TrkIsoVVL_Mu8_TrkIsoVVL_DZ_Mass8_v*
MuonEG	[315252,325172]	HLT_Mu23_TrkIsoVVL_Ele12_CaloIdL_TrackIdL_IsoVL_v*
		HLT_Mu12_TrkIsoVVL_Ele23_CaloIdL_TrackIdL_IsoVL_DZ_v*

Table 1.3: 2018 trigger paths considered for this analysis.

Our analysis relying on the dilepton final state, the single lepton trigger are only considered in order to recover some of the efficiency lost in some cases when one lepton passes the tight identification criteria while the second one does not, and does therefore not trigger the event. The logical *or* of all the trigger paths are usually considered. Eventual events passing several triggers is taken into account as well to make sure to avoid any double counting due to this effect.

These triggers have been studied in order to make sure that they are efficient enough in the p_T region of the leptons of the analysis to avoid any undesired effect due to the turn-on of any trigger. These trigger efficiencies, calculated using a general tag and probe method and found for example for different runs of the 2017 data taking period in Figure 1.1 for a DoubleEG trigger, are then used to reweight the simulated samples.

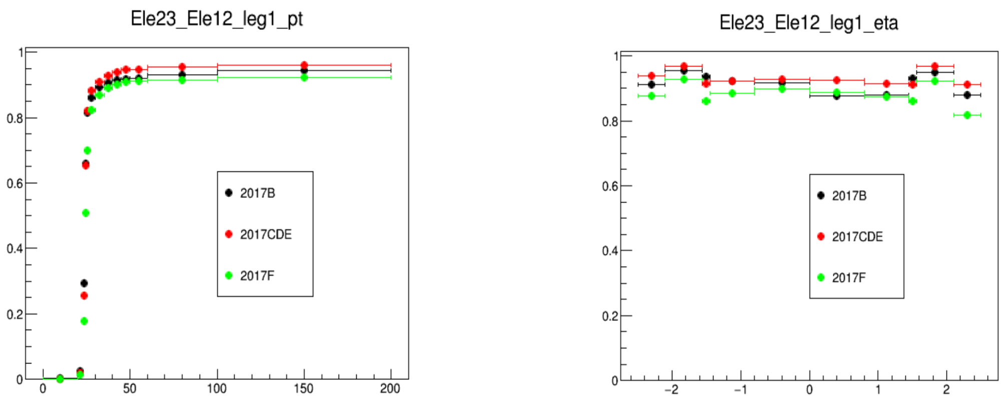

Figure 1.1: DougleEG trigger efficiencies with respect to the p_T (on the left) and η (on the right), computed using a tag and probe method, for the 2017 data taking period.

1.1.2 Electrons selection

Several strategies are used in Compact Muon Solenoid (CMS) in order to be able to identify prompts electrons and isolate this signal over background sources coming mainly from photon conversions, misidentification of jets or electrons coming from the semileptonic decay of the bottom and charm quarks. Several variables, which can be divided in the several following categories, allow to introduce some discrimination between these prompt and fake electrons:

- The **calorimetric observables** use the transverse shape of electromagnetic showers in the Electromagnetic Calorimeter (ECAL), the fact that these electromagnetic showers should be narrower than hadronic showers and the fraction of energy deposited in the Hadronic Calorimeter (HCAL) and in the preshower/endcaps of the ECAL itself for the discrimination. Many different variables belong to this category, such as:
  - **hOverE** $(\frac{H}{E})$, where H corresponds to the energy deposited in the HCAL and E the total energy deposited in the ECAL.
  - **ooEmooP** $\left(\frac{1}{E_{\mathrm{SC}}} - \frac{1}{p}\right)$, where E_{SC} is the Super Cluster (SC) energy and p the momentum of the track at the point of closest approach to the Primary Vertex (PV).
  - **dEtaInSee** $\Delta\eta$ (**dPhiInSee** $\Delta\phi$), the η (ϕ) difference between the SC and the inner track extrapolated from the interaction vertex.
  - **sigmaIetaIeta** ($\sigma_{\eta\eta}$), the weighted cluster Root Mean Square (RMS) inside 5x5 regions of SCs along η.
- The **isolation variables**, requiring the electron candidates to be quite isolated with respect to nearby energetic activity since most of the non-prompt electrons, such as electrons within a jet, are emitted with a large amount of surrounding energy.
  - The **relIsoWithEA** is the main variable that belongs to this category, corresponding to the Particle Flow (PF) isolation defined in a cone of size $\Delta R = 0.3$ around the electron direction and relative to the electron p_T, and taking into account the Pile Up (PU) contamination in this cone.
- The **tracking quality variables**, such as:
  - The **expected inner hits**, the number of pixels without corresponding hits in the trajectory of a reconstructed gsfTrack.
  - The **matched gsfTracks hits**, the χ^2 value calculated from the reconstructed gskTrack and its corresponding hits.
- The **conversion rejection variables**, mostly used to reject most of the photon conversion contamination when defining electrons, using variable such as:
  - The **transverse** d_0 (or d_{xy}) and **longitudinal** d_z **impact parameters**.
  - The **conversion veto**, checking if an electron candidate also matches at least one conversion candidate which also passes the selection cuts.

In this analysis, instead of relying on the four basic Physics Object Group (POG) official Working Points (WPs) (veto, loose, medium and tight) that can be defined with some quality cuts, we rely on the Multi-Variate Analysis (MVA) approach that consists in using a single discriminator variable to perform the discrimination between genuine and misidentified electrons, combining the information coming from more than 20 variables at once using Boosted Decision Trees (BDT).

Two WPs are then given directly by the CMS EGamma POG, corresponding to an electron selection efficiency of 80 and 90% respectively. For this analysis, the tight POG $mva\_90p\_Iso2016$ WP has been chosen for the electron definition, along with additional quality cuts defined in Table 1.4 (as previously mentionned, these cuts sometines differ quite a bit depending on whether the electron interacts with the ECAL barrel ($|\eta| < 1.479$) or one of the endcaps ($|\eta| \geq 1.479$)).

The electron efficiencies computed for this particular selection can be seen in Figure 1.2.

Variable		Barrel cut	Endcap cut
Basic selection			
$\|\eta\|$	$<$	-	2.5
HLT safe selection			
hOverE	$<$	0.060	0.065
ooEmooP	$<$	0.013	0.013
$\|$dEtaInSee $(\Delta\eta)\|$	$<$	0.004	-
$\|$dPhiInSee $(\Delta\phi)\|$	$<$	0.020	-
$\sigma_{\eta\eta}$	$<$	0.011	0.031
ecalPFClusterIso	$<$	0.160	0.120
hcalPFClusterISO	$<$	0.120	0.120
trackIso	$<$	0.08	0.08
GsfTrack χ^2/NDOF	$<$	-	3.0
Additional selection			
lostHits	< 1	< 1	
d_{xy}	< 0.05	< 0.1	
d_z	< 0.1	< 0.2	
pfRelIso03	< 0.0588	< 0.0571	

Table 1.4: Quality cuts applied to define a tight electron in this analysis.

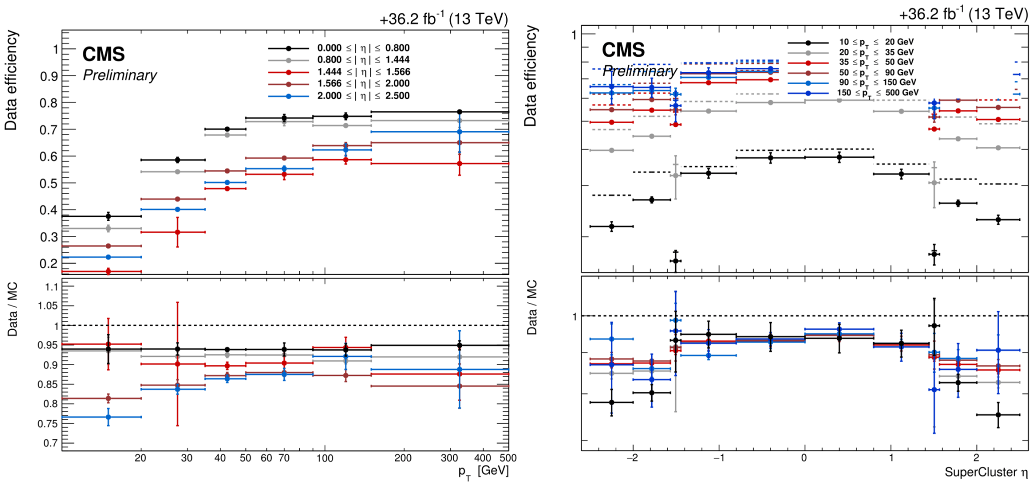

Figure 1.2: Tight electron efficiencies for this analysis, based on the Egamma POG $mva\_90p\_Iso2016$ WP, for the data taking period of 2016.

1.1.3 Muons selection

The selection applied to muons is mostly based on the Muon POG, providing references efficiencies for standard selection, recommendations for the tight selection [120], with a few additional cuts on both the impact parameters.

At the end of the day, a muon can be labeled as **Tight POG** if:

- The PF muon reconstructed is a global muon.
- The χ^2/NDOF of the global muon track fit is less than 10 and at least one muon chamber hit is included in the global muon track fit
- Muon segments in at least two muon stations have been observed.
- Its tracker track has a transverse impact parameter $dxy < 0.2$ cm and a longitudinal impact parameter $d_Z < 0.5$ cm with respect to the PV .
- The number of pixel hits is larger than 0.
- At least 5 tracker layers with hits have been observed.

The selection applied to muons of this particular analysis is a bit tighter though, since the following cuts are applied on top of this selection:

- $p_T > 10$ GeV, $|\eta| < 2.4$ and $|d_z| < 0.1$ cm
- $|d_{xy}| < 0.01$ cm (if $p_T < 20$ GeV) or $|d_{xy}| < 0.02$ cm (if $p_T \geq 20$ GeV)
- Tight muon isolation requirement (< 0.15) with $\Delta\beta$ correction and in a cone size $\Delta R <$ 0.4, as defined in Equation 1.1, in order to reduce the number of muons coming from the hadronization process of bottom and charm quarks.

$$\text{ISO} = \frac{\sum p_T^{\text{ch. had. (PV)}} + \max\left(0, \sum E_T^{\text{neut. had.}} + \sum E_T^{\gamma} - 0.5 \times \sum p_T^{\text{ch. had. (PU)}}\right)}{p_T(\mu)} \tag{1.1}$$

This selection leads to efficiencies higher than 80% for all the muon momenta and pseudorapidities range, as shown in Figure 1.3.

1.1.4 Jet selection

1.2 Signals regions

It is important to note that a strict **blinding policy** has been followed for this search, in order to avoid optimizing the analysis based on what has already seen. The data available to be ploted in the following signal regions has therefore been limited to 1 fb^{-1} for each year.

p_T/η	-2.4:-2.1	-2.1:-1.6	-1.6:-1.2	-1.2:-0.8	-0.8:-0.3	-0.3:-0.2	-0.2:0.0	0.0:0.2	0.2:0.3	0.3:0.8	0.8:1.2	1.2:1.6	1.6:2.1	2.1:2.4
10:15	0.9995	1.0016	0.9985	0.9907	0.9844	1.0183	1.0089	1.0089	1.0265	0.9862	0.9808	0.9882	0.9927	0.9972
15:20	0.9805	0.9870	0.9950	0.9867	0.9935	0.9686	0.9927	0.9927	0.9771	0.9924	0.9826	0.9986	0.9912	0.9797
20:25	0.9756	0.9829	0.9949	0.9823	0.9914	0.9712	0.9906	0.9910	0.9590	0.9917	0.9776	0.9927	0.9873	0.9822
25:30	0.9793	0.9850	0.9942	0.9794	0.9912	0.9659	0.9899	0.9886	0.9610	0.9899	0.9784	0.9932	0.9874	0.9805
30:40	0.9773	0.9828	0.9947	0.9782	0.9891	0.9685	0.9903	0.9883	0.9614	0.9887	0.9770	0.9940	0.9876	0.9828
40:60	0.9766	0.9851	0.9957	0.9796	0.9908	0.9713	0.9911	0.9894	0.9638	0.9898	0.9786	0.9945	0.9871	0.9774
60:100	0.9618	0.9794	0.9963	0.9773	0.9917	0.9597	0.9914	0.9886	0.9655	0.9883	0.9764	0.9948	0.9858	0.9796
100:200	0.9803	0.9743	0.9831	0.9740	0.9949	0.9634	0.9954	0.9814	0.9482	0.9870	0.9732	0.9962	0.9782	0.9895

Color Definition						
Scale Factors	0.99-1.01	0.98-0.99,1.01-1.02	0.97-0.98, 1.02-1.03	0.96-0.97	0.95-0.96	< 0.95

(a) 2016 muon efficiencies

p_T/η	-2.4:-2.1	-2.1:-1.6	-1.6:-1.2	-1.2:-0.8	-0.8:-0.3	-0.3:-0.2	-0.2:0.0	0.0:0.2	0.2:0.3	0.3:0.8	0.8:1.2	1.2:1.6	1.6:2.1	2.1:2.4
10:15	0.9880	0.9827	0.9981	0.9961	1.0018	1.0099	1.0129	1.0129	1.0193	0.9893	0.9767	0.9978	0.9901	0.9852
15:20	0.9735	0.9831	0.9955	0.9849	0.9995	0.9582	0.9932	0.9932	0.9400	0.9891	0.9813	0.9970	0.9899	0.9807
20:25	0.9737	0.9839	0.9976	0.9863	0.9940	0.9561	0.9936	0.9963	0.9757	0.9915	0.9800	0.9975	0.9892	0.9771
25:30	0.9741	0.9819	0.9975	0.9852	0.9931	0.9580	0.9936	0.9952	0.9619	0.9914	0.9790	0.9979	0.9905	0.9826
30:40	0.9719	0.9794	0.9973	0.9842	0.9935	0.9570	0.9932	0.9942	0.9635	0.9921	0.9781	0.9972	0.9900	0.9815
40:60	0.9709	0.9815	0.9979	0.9849	0.9941	0.9556	0.9945	0.9953	0.9636	0.9924	0.9790	0.9966	0.9896	0.9800
60:100	0.9622	0.9779	0.9959	0.9842	0.9935	0.9525	0.9938	0.9944	0.9563	0.9918	0.9747	0.9967	0.9868	0.9887
100:200	0.9649	0.9732	0.9899	0.9851	0.9884	0.9645	1.0060	0.9953	0.9831	0.9872	0.9738	0.9981	0.9868	0.9635

Color Definition						
Scale Factors	0.99-1.01	0.98-0.99	0.97-0.98	0.96-0.97	0.95-0.96	< 0.95

(b) 2017 muon efficiencies

p_T/η	-2.4:-2.1	-2.1:-1.6	-1.6:-1.2	-1.2:-0.8	-0.8:-0.3	-0.3:-0.2	-0.2:0.0	0.0:0.2	0.2:0.3	0.3:0.8	0.8:1.2	1.2:1.6	1.6:2.1	2.1:2.4
10:15	0.9686	0.9806	0.9996	0.9801	0.9975	0.9895	1.0053	1.0053	0.9446	0.9908	0.9763	0.9984	0.9967	0.9726
15:20	0.9683	0.9817	0.9974	0.9836	0.9951	0.9513	0.9925	0.9925	0.9678	0.9901	0.9849	0.9945	0.9888	0.9810
20:25	0.9681	0.9826	0.9979	0.9874	0.9963	0.9670	0.9936	0.9986	0.9725	0.9921	0.9835	0.9967	0.9899	0.9786
25:30	0.9679	0.9821	0.9977	0.9858	0.9960	0.9779	0.9943	0.9918	0.9795	0.9941	0.9804	0.9964	0.9890	0.9742
30:40	0.9688	0.9789	0.9970	0.9848	0.9956	0.9778	0.9933	0.9946	0.9740	0.9930	0.9814	0.9957	0.9885	0.9749
40:60	0.9672	0.9802	0.9967	0.9856	0.9964	0.9752	0.9950	0.9952	0.9743	0.9943	0.9821	0.9958	0.9875	0.9761
60:100	0.9652	0.9756	0.9959	0.9835	0.9957	0.9725	0.9919	0.9946	0.9760	0.9931	0.9803	0.9945	0.9853	0.9702
100:200	0.9500	0.9750	0.9944	0.9839	0.9976	0.9688	0.9984	0.9890	0.9460	0.9925	0.9778	0.9954	0.9780	0.9881

Color Definition						
Scale Factors	0.99-1.01	0.98-0.99	0.97-0.98	0.96-0.97	0.95-0.96	< 0.95

(c) 2018 muon efficiencies

Figure 1.3: Tight muon efficiencies for this analysis, based on the Muon POG tight WP with additional cuts for 2016, 2017 and 2018.

1.3 Control regions

Different control regions have been defined in order for the validity of the simulations performed for the different SM processes.

1.3.1 Same sign control region

A same sign control region has been defined in order to check the non-prompt background, calculated using a data-driven tight-to-loose method described in Section **??**. This CR is defined with the following cuts:

- Exactly 2 same sign leptons
- $p_{T,1} > 20$ (25) GeV for e (μ)
- $p_{T,2} > 13$ GeV
- $|\eta| < 2.5$ for both leptons
- $m_{ll} > 12$ GeV
- PuppiMET > 20 GeV
- $p_T^{ll} > 30$ GeV
- mth > 60 GeV

Several regions are then defined according to this cut, depending on the data taking period, on the channel, on the number of jets observed and on the p_T of the second lepton. Some plots can be found in Figure 1.4.

In order to cover for most of the discrepancies between the data and the simulation observed in the distributions of this control region, a flat 30% systematic uncertainty is typically associated to this background, as will be discussed in more details in Section 2.1.

1.4 Background-signal discrimination

1.4.1 Discriminating variables

Missing Transverse Energy (MET)

This variable has already been defined in Section **??**, and corresponds to the imbalance in transverse momentum which can be left by different phenomena, such as the apparition of a SM neutrino or the existence of DM particles, able to escape the detector without being detected.

This variable is expected to induce some discrimination between the signal and the backgrounds because, even tough the $t\bar{t}$ in the dilepton final state is expected to produce two neutrinos and therefore some MET, the $t\bar{t}$+DM signal model is expected to have mostly the same contribution to the MET from its own two neutrinos, and an additional contributions from the pair $\chi\bar{\chi}$ produced. The MET spectrum is therefore expected to reach higher values for the signal than the backgrounds.

TALK ABOUT SINGLE TOP?

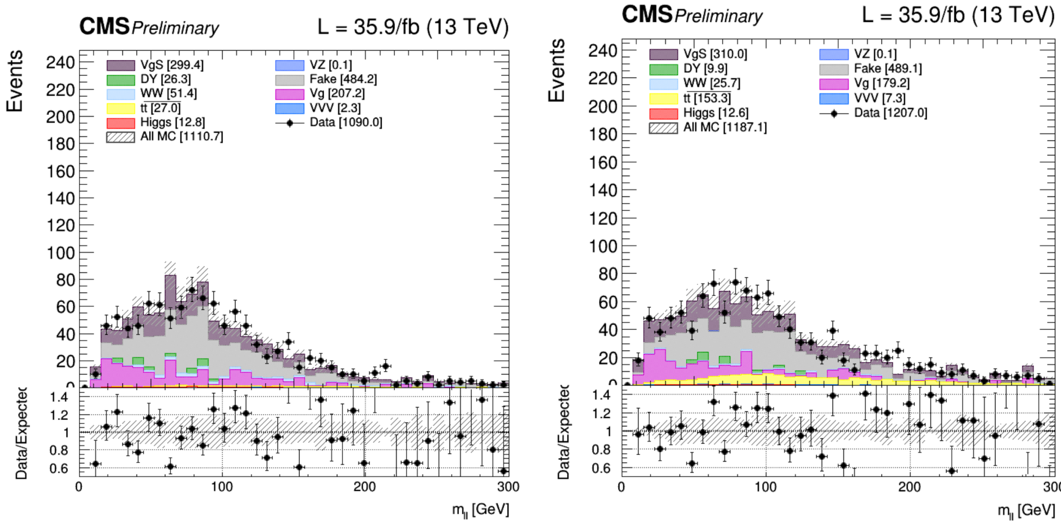

(a) 2016 same sign control plots

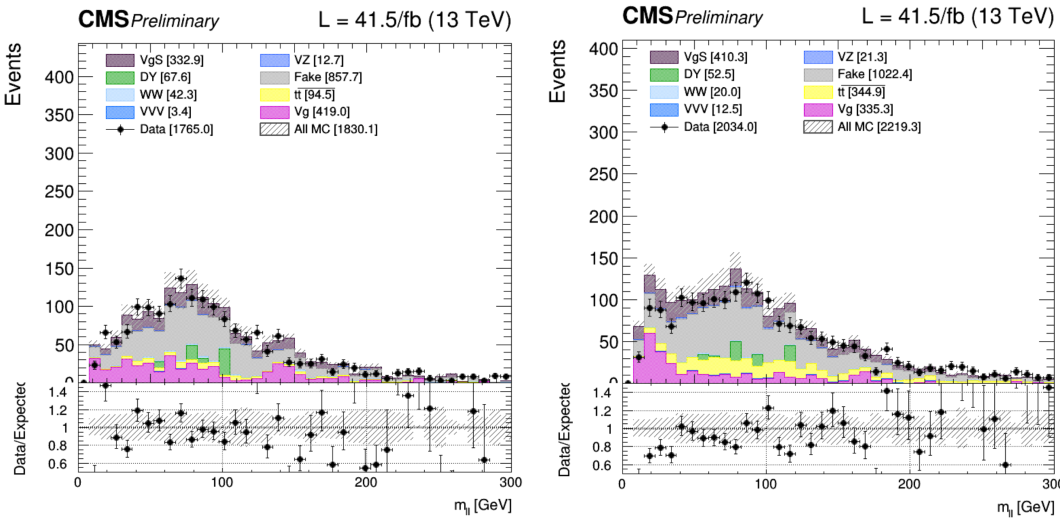

(b) 2017 same sign control plots

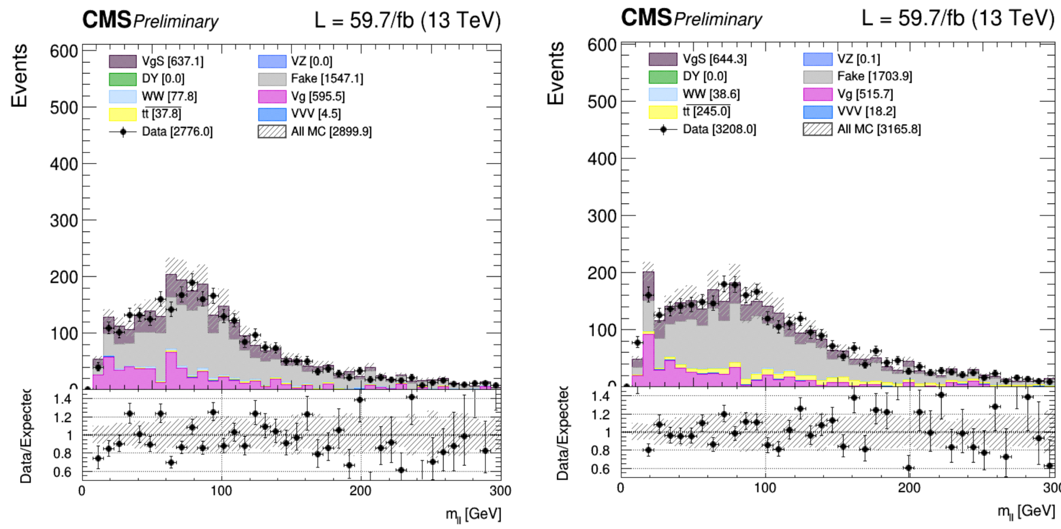

(c) 2018 same sign control plots

Figure 1.4: Same sign control region m_{ll} distributions for the years 2016, 2017 and 2018 and for the $e\mu$ channel and for the 0-jet (on the left) and 1j (on the right) categories.

Stransverse mass

The m_{T2} variable, also called **stransverse mass**, is an extension of the definition of the transverse mass m_T to cases when pairs of particles with the same flavor decay into one visible and one invisible particle, such as what happens in the $W \to l\nu$ decay, for example.

In this particular case, two particles contribute to the presence of Missing Transverse Energy (MET) and the individual contribution of each particle ($\not{\boldsymbol{p}}_{\boldsymbol{T_1}}$ and $\not{\boldsymbol{p}}_{\boldsymbol{T_2}}$) to this missing energy cannot be inferred. The stransverse mass is then defined according to Equation 1.2, where $\boldsymbol{p_{T_i}} = \overrightarrow{p_{T_i}}$ is the (visible) transverse momentum of the particle i and α is the angle between the visible and invisible p_T of the decay considered [114].

$$\begin{cases} M_{T2}^2 = \min\limits_{\not{\boldsymbol{p}}_{\boldsymbol{T_1}} + \not{\boldsymbol{p}}_{\boldsymbol{T_2}} = \not{\boldsymbol{p}}_{\boldsymbol{T}_{\mathrm{tot}}}} \left(\max \left(m_T^2(\boldsymbol{p_{T_1}}, \not{\boldsymbol{p}}_{\boldsymbol{T_1}}), m_T^2(\boldsymbol{p_{T_2}}, \not{\boldsymbol{p}}_{\boldsymbol{T_2}}) \right) \right) \\ m_T^2(\boldsymbol{p_T}, \not{\boldsymbol{p}}_{\boldsymbol{T}}) = 4\ |\boldsymbol{p_T}||\not{\boldsymbol{p}}_{\boldsymbol{T}}|\ \sin^2\left(\frac{\alpha}{2}\right) \end{cases} \tag{1.2}$$

This equation can be understood in the following way: to compute the m_{T2} variable, different combinations ($\not{\boldsymbol{p}}_{\boldsymbol{T_1}}$, $\not{\boldsymbol{p}}_{\boldsymbol{T_2}}$) satisfying the condition $\not{\boldsymbol{p}}_{\boldsymbol{T_1}} + \not{\boldsymbol{p}}_{\boldsymbol{T_2}} = \not{\boldsymbol{p}}_{\boldsymbol{T}_{\mathrm{tot}}}$ need to be probed, keeping only the combination which results in the lowest value.

In this particular analysis, $M_{T2}(ll)$ is calculated, since the role of the visible particles is played by the two final state leptons. This variable is expected to introduce some discrimination because, according to the definition just given, the $M_{T2}(ll)$ variable for a SM $t\bar{t}$ process is expected to have an endpoint exactly at the mass of the W boson, while an eventual $t\bar{t}$+DM signal does not have this limitation in the $M_{T2}(ll)$ spectrum because of the pair of DM particles produced, which also contributes to the total MET of the event.

However, in practice, we do observe a tail in this spectrum even for SM $t\bar{t}$ without DM, because of the instrumental MET sometimes observed or the fact that some selected leptons are not actually prompt leptons but can be jets misidentified as leptons by the detector.

TALK ABOUT SINGLE TOP?

1.4.2 Neural network

Chapter 2

Results and interpretations

2.1 Systematics and uncertainties

2.2 Results

Chapter 3

Conclusions

3.1 Future prospects

Appendices

Appendix A

Samples used

A.1 Data samples

All the data samples considered for this analysis are listed in Tables A.1, A.2 and A.3. The luminosity of each dataset has been computed using the Brilcalc tool provided by CMS [121], while the number of generated events has been obtained using the CERN official Data Aggregation System (DAS).

A.2 Signal samples

To be completed once the files are actually available

A.3 Backgrounds samples

To be completed once the analysis actually performed LO/NLO Generator used

Dataset	Events (size)	$\mathcal{L}$ [fb^{-1}]
Run 2016B		
/DoubleEG/Run2016B_ver2-Nano1June2019_ver2-v1/NANOAOD	143073268 (99.4Gb)	
/DoubleMuon/Run2016B_ver2-Nano1June2019_ver2-v1/NANOAOD	82535526 (53.2Gb)	
/MuonEG/Run2016B_ver2-Nano1June2019_ver2-v1/NANOAOD	32727796 (26.8Gb)	5.8
/SingleElectron/Run2016B_ver2-Nano1June2019_ver2-v1/NANOAOD	246440440 (167.8Gb)	
/SingleMuon/Run2016B_ver2-Nano1June2019_ver2-v1/NANOAOD	158145722 (96.4Gb)	
Run 2016C		
/DoubleEG/Run2016C-Nano1June2019-v1/NANOAOD	47677856 (35.3Gb)	
/DoubleMuon/Run2016C-Nano1June2019-v1/NANOAOD	27934629 (19.7Gb)	
/MuonEG/Run2016C-Nano1June2019-v1/NANOAOD	15405678 (12.8Gb)	2.6
/SingleElectron/Run2016C-Nano1June2019-v1/NANOAOD	97259854 (69.3Gb)	
/SingleMuon/Run2016C-Nano1June2019-v1/NANOAOD	67441308 (42.4Gb)	
Run 2016D		
/DoubleEG/Run2016D-Nano1June2019-v1/NANOAOD	53324960 (39.6Gb)	
/DoubleMuon/Run2016D-Nano1June2019-v1/NANOAOD	33861745 (24.1Gb)	
/MuonEG/Run2016D-Nano1June2019-v1/NANOAOD	23482352 (19.4Gb)	4.2
/SingleElectron/Run2016D-Nano1June2019-v1/NANOAOD	148167727 (104.4Gb)	
/SingleMuon/Run2016D-Nano1June2019-v1/NANOAOD	98017996 (61.3Gb)	
Run 2016E		
/DoubleEG/Run2016E-Nano1June2019-v1/NANOAOD	49877710 (37.9Gb)	
/DoubleMuon/Run2016E-Nano1June2019-v1/NANOAOD	28246946 (20.8Gb)	
/MuonEG/Run2016E-Nano1June2019-v2/NANOAOD	22519303 (19.0Gb)	4.0
/SingleElectron/Run2016E-Nano1June2019-v1/NANOAOD	117321545 (86.5Gb)	
/SingleMuon/Run2016E-Nano1June2019-v1/NANOAOD	90984718 (58.7Gb)	
Run 2016F		
/DoubleEG/Run2016F-Nano1June2019-v1/NANOAOD	34577629 (26.9Gb)	
/DoubleMuon/Run2016F-Nano1June2019-v1/NANOAOD	20329921 (15.3Gb)	
/MuonEG/Run2016F-Nano1June2019-v1/NANOAOD	16002165 (13.6Gb)	3.1
/SingleElectron/Run2016F-Nano1June2019-v1/NANOAOD	70593532 (51.4Gb)	
/SingleMuon/Run2016F-Nano1June2019-v1/NANOAOD	65489554 (42.4Gb)	
Run 2016G		
/DoubleEG/Run2016G-Nano1June2019-v1/NANOAOD	78797031 (61.6Gb)	
/DoubleMuon/Run2016G-Nano1June2019-v1/NANOAOD	45235604 (34.2Gb)	
/MuonEG/Run2016G-Nano1June2019-v1/NANOAOD	33854612 (29.0Gb)	7.6
/SingleElectron/Run2016G-Nano1June2019-v1/NANOAOD	153363109 (109.2Gb)	
/SingleMuon/Run2016G-Nano1June2019-v1/NANOAOD	149912248 (94.6Gb)	
Run 2016H		
/DoubleEG/Run2016H-Nano1June2019-v1/NANOAOD	85388734 (67.7Gb)	
/DoubleMuon/Run2016H-Nano1June2019-v1/NANOAOD	48912812 (37.3Gb)	
/MuonEG/Run2016H-Nano1June2019-v1/NANOAOD	29236516 (26.0Gb)	8.6
/SingleElectron/Run2016H-Nano1June2019-v1/NANOAOD	128854598 (93.8Gb)	
/SingleMuon/Run2016H-Nano1June2019-v1/NANOAOD	174035164 (110.2Gb)	

Table A.1: Datasets collected in 2016 and considered for this analysis.

Dataset	Events (size)	$\mathcal{L}$ [fb^{-1}]
Run 2017B		
/DoubleEG/Run2017B-Nano1June2019-v1/NANOAOD	58088760 (46.6Gb)	
/DoubleMuon/Run2017B-Nano1June2019-v1/NANOAOD	14501767 (10.8Gb)	
/SingleElectron/Run2017B-Nano1June2019-v1/NANOAOD	60537490 (42.2Gb)	4.8
/SingleMuon/Run2017B-Nano1June2019-v1/NANOAOD	136300266 (86.2Gb)	
/MuonEG/Run2017B-Nano1June2019-v1/NANOAOD	4453465 (4.1Gb)	
Run 2017C		
/DoubleEG/Run2017C-Nano1June2019-v1/NANOAOD	65181125 (53.8Gb)	
/DoubleMuon/Run2017C-Nano1June2019-v1/NANOAOD	49636525 (39.5Gb)	
/SingleElectron/Run2017C-Nano1June2019-v1/NANOAOD	136637888 (102.5Gb)	9.7
/SingleMuon/Run2017C-Nano1June2019-v1/NANOAOD	165652756 (109.5Gb)	
/MuonEG/Run2017C-Nano1June2019-v1/NANOAOD	15595214 (15.0Gb)	
Run 2017D		
/DoubleEG/Run2017D-Nano1June2019-v1/NANOAOD	25911432 (21.6Gb)	
/DoubleMuon/Run2017D-Nano1June2019-v1/NANOAOD	23075733 (18.6Gb)	
/SingleElectron/Run2017D-Nano1June2019-v1/NANOAOD	51526710 (38.5Gb)	4.2
/SingleMuon/Run2017D-Nano1June2019-v1/NANOAOD	70361660 (47.2Gb)	
/MuonEG/Run2017D-Nano1June2019-v1/NANOAOD	9164365 (8.9Gb)	
Run 2017E		
/DoubleEG/Run2017E-Nano1June2019-v1/NANOAOD	56233597 (49.8Gb)	
/DoubleMuon/Run2017E-Nano1June2019-v1/NANOAOD	51589091 (44.4Gb)	
/SingleElectron/Run2017E-Nano1June2019-v1/NANOAOD	102121689 (81.3Gb)	9.3
/SingleMuon/Run2017E-Nano1June2019-v1/NANOAOD	154630534 (111.0Gb)	
/MuonEG/Run2017E-Nano1June2019-v1/NANOAOD	19043421 (19.2Gb)	
Run 2017F		
/DoubleEG/Run2017F-Nano1June2019-v1/NANOAOD	74307066 (67.1Gb)	
/DoubleMuon/Run2017F-Nano1June2019-v1/NANOAOD	79756560 (68.0Gb)	
/SingleElectron/Run2017F-Nano1June2019-v1/NANOAOD	128467223 (105.2Gb)	13.5
/SingleMuon/Run2017F-Nano1June2019-v1/NANOAOD	242135500 (178.3Gb)	
/MuonEG/Run2017F-Nano1June2019-v1/NANOAOD	25776363 (26.3Gb)	

Table A.2: Datasets collected in 2017 and considered for this analysis.

Dataset	Events (size)	$\mathcal{L}$ [fb^{-1}]
Run 2018A		
/DoubleMuon/Run2018A-Nano25Oct2019-v1/NANOAOD	75499908 (62.6Gb)	13.5
/EGamma/Run2018A-Nano25Oct2019-v1/NANOAOD	327843843 (261.8Gb)	
/SingleMuon/Run2018A-Nano25Oct2019-v1/NANOAOD	241608232 (167.7Gb)	
/MuonEG/Run2018A-Nano25Oct2019-v1/NANOAOD	32958503 (32.3Gb)	
Run 2018B		
/DoubleMuon/Run2018B-Nano25Oct2019-v1/NANOAOD	35057758 (28.3Gb)	6.8
/EGamma/Run2018B-Nano25Oct2019-v1/NANOAOD	153822427 (123.1Gb)	
/SingleMuon/Run2018B-Nano25Oct2019-v1/NANOAOD	119918017 (82.3Gb)	
/MuonEG/Run2018B-Nano25Oct2019-v1/NANOAOD	16211567 (15.8Gb)	
Run 2018C		
/DoubleMuon/Run2018C-Nano25Oct2019-v1/NANOAOD	34565869 (27.6Gb)	6.6
/EGamma/Run2018C-Nano25Oct2019-v1/NANOAOD	147827904 (119.2Gb)	
/SingleMuon/Run2018C-Nano25Oct2019-v1/NANOAOD	110032072 (75.7Gb)	
/MuonEG/Run2018C-Nano25Oct2019-v1/NANOAOD	15652198 (15.3Gb)	
Run 2018D		
/DoubleMuon/Run2018D-Nano25Oct2019_ver2-v1/NANOAOD	168605834 (128.6Gb)	32.0
/EGamma/Run2018D-Nano25Oct2019-v1/NANOAOD	751348648 (583.6Gb)	
/SingleMuon/Run2018D-Nano25Oct2019-v1/NANOAOD	513867253 (344.5Gb)	
/MuonEG/Run2018D-Nano25Oct2019_ver2-v1/NANOAOD	71961587 (68.6Gb)	

Table A.3: Datasets collected in 2018 and considered for this analysis.

Appendix B

Neural network optimization

List of figures

1.1 DougleEG trigger efficiencies with respect to the p_T (on the left) and η (on the right), computed using a tag and probe method, for the 2017 data taking period. . 3

1.2 Tight electron efficiencies for this analysis, based on the Egamma POG $mva\_90p\_Iso2016$ WP, for the data taking period of 2016. 5

1.3 Tight muon efficiencies for this analysis, based on the Muon POG tight WP with additional cuts for 2016, 2017 and 2018. 7

1.4 Same sign control region m_{ll} distributions for the years 2016, 2017 and 2018 and for the $e\mu$ channel and for the 0-jet (on the left) and 1j (on the right) categories. . . . 9

List of tables

1.1 2016 trigger paths considered for this analysis. 2

1.2 2017 trigger paths considered for this analysis. 2

1.3 2018 trigger paths considered for this analysis. 3

1.4 Quality cuts applied to define a tight electron in this analysis. 5

A.1 Datasets collected in 2016 and considered for this analysis. 18

A.2 Datasets collected in 2017 and considered for this analysis. 19

A.3 Datasets collected in 2018 and considered for this analysis. 20

Bibliography

[1] F. Englert and R. Brout, ”Broken symmetry and the mass of gauge vector mesons”, Phys. Rev. Lett. 13, pp. 321-323, 1964

[2] P. W. Higgs, ”Broken symmetries and the masses of gauge bosons”, Phys. Rev. Lett. 13, pp. 508-509, 1964

[3] S. Chatrchyan et al., ”Observation of a new boson at a mass of 125 GeV with the CMS experiment at the LHC”, Phys. Lett. B716, pp. 30-61, 2012 [arXiv: 1207.7235]

[4] G. Aad et al., ”Observation of a new particle in the search for the Standard Model Higgs boson with the ATLAS detector at the LHC”, Phys. Lett. B716, pp. 1-29, 2012 [arXiv: 1207.7214]

[5] V.C. Rubin, W.K. Ford and N. Thonnard, ”Rotational properties of 21 SC galaxies with a large range of luminosities and radii, from NGC 4605 (R=4kpc) to UGC 2885 (R=122kpc)”, Astrophysical Journal 238, pp. 471-487, 1980

[6] K.G. Begeman, A.H. Broeils and R.H. Sanders, ”Extended rotation curves of spiral galaxies - Dark haloes and modified dynamics”, Monthly Notices of the Royal Astronomical Society, vol. 249, issue 3, ISSN 0035-8711, 1991

[7] A. Robertson, R. Massey and V. Eke, ”What does the Bullet Cluster tell us about self-interacting dark matter?”, Monthly Notices of the Royal Astronomical Society, vol. 465, issue 1, 2017 [arXiv: 1605.04307]

[8] J.B. Mu?oz, C. Dvorkin and A. Loeb, ”21-cm Fluctuations from Charged Dark Matter”, Phys. Rev. Lett. 121, 121301 (2018) [arXiv: 1804.01092]

[9] A. Natarajan, ”A closer look at CMB constraints on WIMP dark matter”, Phys. Rev. D85, 2012 [arXiv:1201.3939]

[10] G. D’Ambrosio G.F. Giudice, G. Isidori and A. Strumia, ”Minimal Flavour Violation: an effective field theory approach”, Nucl.Phys. 645, pp 155-187, 2002 [arXiv:0207.036]

[11] CMS Collaboration, ”Search for the production of dark matter in association with top-quark pairs in the single-lepton final state in proton-proton collisions at $\sqrt{s} = 8$ TeV”, JHEP, vol. 6 121, 2015

[12] CMS Collaboration,, ”Search for the Production of Dark Matter in Association with Top Quark Pairs in the Di-lepton Final State in pp collisions at $\sqrt{s} = 8$ TeV”, CMS-PAS-B2G-13-004, 2014

[13] ”Search for dark matter in events with heavy quarks and missing transverse momentum in pp collisions with the ATLAS detector”, Eur. Phys. J. C (2015) 75:92

[14] ATLAS Collaboration, Search for the Supersymmetric Partner of the Top Quark in the Jets+Emiss Final State at $\sqrt{s} = 13$ TeV”, ATLAS-CONF-2016-077

[15] ATLAS Collaboration, ”Search for top squarks in final states with one isolated lepton, jets, and missing transverse momentum in $\sqrt{s} = 13$ TeV pp collisions with the ATLAS detector”, ATLAS-CONF-2016-050, 2016

[16] ATLAS Collaboration, ”Search for direct top squark pair production and dark matter production in final states with two leptons in $\sqrt{s} = 13$ TeV pp collisions using 13.3 fb^{-1} of ATLAS data”, ATLAS-CONF-2016-076, 2016

[17] ATLAS Collaboration, ”Search for dark matter produced in association with bottom or top quarks in $\sqrt{s} = 13$ TeV pp collisions with the ATLAS detector”, Eur. Phys. J. C 78 (2018) 18 [arXiv: 1710.11412]

[18] CMS Collaboration, Search for dark matter produced in association with heavy-flavor quark pairs in proton-proton collisions at $\sqrt{s} = 13$ TeV”, Eur. Phys. J. C (2017) 77: 845

[19] CMS Collaboration, ”Search for dark matter particles produced in association with a top quark pair at $\sqrt{s} = 13$ TeV”, Phys. Rev. Lett. 122, 011803 (2019) [arXiv: 1807.06522]

[20] CMS Collaboration, ”Search for dark matter produced in association with a single top quark or a top quark pair in proton-proton collisions at $\sqrt{s} = 13$ TeV”, JHEP, vol. 03 141, 2019 [arXiv: 1901.01553]

[21] S. Manzoni, ”The Standard Model and the Higgs Boson”, Physics with Photons Using the ATLAS Run 2 Data, Springer Theses, 2019

[22] A.B. Balantekin, A. Gouvea and B.Kayser, ”Addressing the Majorana vs. Dirac Question with Neutrino Decays”, FERMILAB-PUB-18-418-T, NUHEP-TH/18-09 [arXiv: 1808.10518]

[23] J. Woithe, G.J. Wiener and F. Van der Vecken, ”Let’s have a coffee with the Standard Model of particle physics!”, Physics education 52, number 3, 2017

[24] F. Zwicky, ”Die Rotverschiebung von extragalaktischen Nebeln”, Helvetica Physica Acta , vol. 6, pp. 110-127, 1933

[25] S. Van den Bergh,Phys Rev D ”The early history of dark matter”, Dominion Astrophysical Observatory, 1999

[26] V.C. Rubin, W.K. Ford, ”Rotation of the Andromeda Nebula from a Spectroscopic Survey of Emission Regions”, Astrophysical Journal 159, p. 379, 1970

[27] A. A. Penzias, R.W. Wilson, ”A Measurement of Excess Antenna Temperature at 4080 Mc/s”, Astrophysical Journal 142, pp. 419-421

[28] D.J. Fixsen, ”The temperature of the cosmic microwave background”, Astrophysical Journal, 2009

[29] Planck Collaboration, ”Planck 2018 results. I. Overview and the cosmological legacy of Planck”, 2018 [arXiv: 1807.06205]

[30] R. Tojeiro, ”Understanding the Cosmic Microwave Background Temperature Power Spectrum”, 2006

[31] Planck Collaboration, ”Planck 2018 results. VI. Cosmological parameters”, 2018 [arXiv: 1807.06209]

[32] ”Astrophysical Constants and Parameters”, 2019

[33] D. Clowe et all., ”A Direct Empirical Proof of the Existence of Dark Matter”, Astrophysical Journal Letters 648, 2006

[34] K.R. Dienes, J. Fennick, J. Kumar, B. Thomas "Dynamical Dark Matter from Thermal Freeze-Out", Phys. Rev. D 97, 063522 (2018) [arXiv: 1712.09919]

[35] C.S. Frenk, S.D.M. White, "Dark matter and cosmic structure", Annalen der Physik, p. 22 , 2012 [arXiv: 1210.0544]

[36] R. Kirk, "Dark matter genesis"

[37] M. Drewes et all., "A White Paper on keV Sterile Neutrino Dark Matter", 2016 [arXiv: 1602.04816]

[38] C. Alcock et all., "The MACHO Project: Microlensing Results from 5.7 Years of LMC Observations", Astrophys.J. 542 (2000) 281-307

[39] P. Tisserand et all., "Limits on the Macho content of the Galactic Halo from the EROS-2 Survey of the Magellanic Clouds", A & A 469, pp. 387-404 (2007)

[40] EROS and MACHO collaborations, "EROS and MACHO Combined Limits on Planetary Mass Dark Matter in the Galactic Halo", 1998

[41] Particle Data Group, "Neutrino Cross Section Measurements", PDG 2019

[42] K. McFarland, "Neutrino Interactions", 2008 [arXiv: 0804.3899]

[43] E. Morgante, "Aspects of WIMP Dark Matter Searches at Colliders and Other Probes", Springer theses, 2016

[44] F. Couchot et all., "Cosmological constraints on the neutrino mass including systematic uncertainties", A & A 606, A104 (2017)

[45] E. Bulbul et all., "Detection of An Unidentified Emission Line in the Stacked X-ray spectrum of Galaxy Clusters", 2014 [arXiv: 1402.2301]

[46] A. Boyarsky et all., "An unidentified line in X-ray spectra of the Andromeda galaxy and Perseus galaxy cluster", Phys. Rev. Lett. 113, 251301 (2014) [arXiv: 1402.4119]

[47] A. Boyarsky et all., "Checking the dark matter origin of 3.53 keV line with the Milky Way center", Phys. Rev. Lett. 115, 161301 (2015) [arXiv: 1408.2503]

[48] T. Jeltema1 and S.Profumo, "Deep XMM Observations of Draco rule out at the 99% Confidence Level a Dark Matter Decay Origin for the 3.5 keV Line", 2015 [arXiv: 1512.01239]

[49] D. Wu, "A Brief Introduction to the Strong CP Problem", Superconducting Super Collider Laboratory, 1991

[50] R.D. Peccei, H.R. Quinn, "CP Conservation in the Presence of Pseudoparticles", Phys. Rev. Lett. 38, 1440, 1977

[51] P.W. Graham et all., "Experimental Searches for the Axion and Axion-like Particles", Annual Review if Nuclear and Particle Science 65, 2015 [arXiv: 1602.00039]

[52] CAST collaboration, "New CAST limit on the axion-photon interaction", Nature Physics 13, pp. 584-590 (2017)

[53] B. Penning, "The Pursuit of Dark Matter at Colliders - An Overview", 2017 [arXiv: 1712.01391]

[54] M. Schumann, "Direct Detection of WIMP Dark Matter: Concepts and Status", J. Phys. G46 (2019) no.10, 103003 [arXiv: 1903.03026]

[55] S.C. Martin et all., "The RAVE survey: constraining the local Galactic escape speed", Mon.Not.Roy.Astron.Soc.379:755-772, 2007

[56] K. Freese, M. Lisanti, C. Savage, "Annual Modulation of Dark Matter: A Review", [arXiv: 1209.3339v3]

[57] T.M. Undagoitia and L. Rauch, "Dark matter direct-detection experiments", J. Phys. G43 (2016) no.1, 013001 [arXiv: 1509.08767]

[58] R. Bernabei et all., "First results from DAMA/LIBRA and the combined results with DAMA/NaI", Eur.Phys.J.C56:333-355, 2008 [arXiv: 0804.2741]

[59] J.M. Gaskins, "A review of indirect searches for particle dark matter", Contemporary Physics, 2016 [arXiv: 1604.00014]

[60] F.S. Queiroz, "Dark Matter Overview: Collider, Direct and Indirect Detection Searches", Max-Planck Institute of Physics

[61] LAT collaboration, "Constraints on Dark Matter Annihilation in Clusters of Galaxies with the Fermi Large Area Telescope", JCAP 05(2010)025 [arXiv: 1002.2239]

[62] A.A. Moiseev et all., "Dark Matter Search Perspectives with GAMMA-400", 2013 [arXiv: 1307.2345]

[63] L. Covi et all., "Neutrino Signals from Dark Matter Decay", JCAP 1004:017, 2010 [arXiv: 0912.3521]

[64] B. Lu and H. Zong, "Limits on the Dark Matter from AMS-02 antiproton and positron fraction data", Phys. Rev. D 93, 103517 (2016) [arXiv: 1510.04032]

[65] J. Abdallah et all., "Simplified Models for Dark Matter Searches at the LHC", Phys. Dark Univ. 9-10 (2015) 8-23 [arXiv: 1506.03116]

[66] H. An, L. Wang, H. Zhang, "Dark matter with t-channel mediator: a simple step beyond contact interaction", Phys. Rev. D 89, 115014 (2014) [arXiv: 1308.0592]

[67] ATLAS Collaboration, "Search for dark matter and other new phenomena in events with an energetic jet and large missing transverse momentum using the ATLAS detector", JHEP 01 (2018) 126 [arXiv: 1711.03301]

[68] CMS Collaboration, "Search for new physics in the monophoton final state in proton-proton collisions at $\sqrt{s} = 13$ TeV", J. High Energy Phys. 10 (2017) 073 [arXiv: 1706.03794]

[69] CMS Collaboration, "Search for dark matter produced with an energetic jet or a hadronically decaying W or Z boson at $\sqrt{s} = 13$ TeV", JHEP 07 (2017) 014 [arXiv: 1703.01651]

[70] CMS Collaboration, "Search for new physics in final states with an energetic jet or a hadronically decaying W or Z boson and transverse momentum imbalance at $\sqrt{s} = 13$ TeV", Phys. Rev. D 97, 092005 (2018) [arXiv: 1712.02345]

[71] ATLAS Collaboration, "Search for dark matter in association with a Higgs boson decaying to two photons at $\sqrt{s} = 13$ TeV with the ATLAS detector", Phys. Rev. D 96 (2017) 112004 [arXiv: 1706.03948]

[72] CMS Collaboration, "Search for associated production of dark matter with a Higgs boson decaying to $b\bar{b}$ or $\gamma\gamma$ at $\sqrt{s} = 13$ TeV", JHEP 10 (2017) 180 [arXiv: 1703.05236]

[73] Atlas Collaboration, "Search for new phenomena in dijet events using 37 fb$^{?1}$ of pp collision data collected at $\sqrt{s} = 13$ TeV with the ATLAS detector", Phys. Rev. D 96, 052004 (2017) [arXiv: 1703.09127]

[74] CMS Collaboration, "Search for narrow and broad dijet resonances in proton-proton collisions at $\sqrt{s} = 13$ TeV and constraints on dark matter mediators and other new particles", JHEP 08 (2018) 130 [arXiv: 1806.00843]

[75] C. Munoz, "Models of Supersymmetry for Dark Matter", FTUAM 17/2, IFT-UAM/CSIC-17-005, 2017 [arXiv: 1701.05259]

[76] CMS Collaboration, "Searches for invisible decays of the Higgs boson in pp collisions at $sqrts =$ 7, 8, and 13 TeV", JHEP 02 (2017) 135 [arXiv: 1610.09218]

[77] J. Alimena et all., "Searching for long-lived particles beyond the Standard Model at the Large Hadron Collider", 2019 [arXiv: 1903.04497]

[78] A. Albert et all., "Recommendations of the LHC Dark Matter Working Group: Comparing LHC searches for heavy mediators of dark matter production in visible and invisible decay channels", 2017 [arXiv: 1703.05703]

[79] M. Tanabashi et al., Particle Data Group, Phys. Rev. D98, 030001 (2018)

[80] R. Schicker, "The ALICE detector at LHC", 2005

[81] LHCb Collaboration, "LHCb Detector Performance", Int. J. Mod. Phys. A 30, 1530022 (2015) [arXiv: 1412.6352]

[82] J.T. Boyd, "LHC Run-2 and Future Prospects", 2020

[83] E. Gschwendtner, "AWAKE, A Particle-driven Plasma Wakefield Acceleration Experiment", CERN Yellow Report CERN 2016-001, pp.271-288 [arXiv: 1705.10573]

[84] M. Thomson, "Modern Particle Physics", Cambridge University Press, 2013

[85] G. Apollinari et all., "High Luminosity Large Hadron Collider HL-LHC", CERN Yellow Report CERN-2015-005, pp.1-19 [arXiv: 1705.08830]

[86] CMS Collaboration, "The CMS experiment at the CERN LHC", JINST 3 (2008) S08004

[87] CMS Collaboration, "Precision measurement of the structure of the CMS inner tracking system using nuclear interactions", JINST 13 (2018) P10034 [arXiv: 1807.03289]

[88] M.S. Kim, "CMS reconstruction improvement for the muon tracking by the RPC chambers", 2013 JINST 8 T03001 [arXiv: 1209.2646]

[89] CMS Collaboration, "Performance of the CMS muon detector and muon reconstruction with proton-proton collisions at $\sqrt{s} = 13$ TeV", JINST 13 (2018) P06015 [arXiv: 1804.04528]

[90] CMS Collaboration, "Particle-Flow Event Reconstruction in CMS and Performance for Jets, Taus, and MET", CMS-PAS-PFT-09-001, 2009

[91] CMS Collaboration, "Description and performance of track and primary-vertex reconstruction with the CMS tracker", JINST 9 (2014) P10009 [arXiv: 1405.6569]

[92] V. Knunz, "Measurement of Quarkonium Polarization to Probe QCD at the LHC", Springer theses, 2015

[93] CMS Collaboration, "Performance of electron reconstruction and selection with the CMS detector in proton-proton collisions at $\sqrt{s} = 8$ TeV", JINST 10 (2015) P06005 [arXiv: 1502.02701]

[94] J. Rembser, "CMS Electron and Photon Performance at 13 TeV", J. Phys. Conf. Ser. 1162 012008, 2019

[95] P.L.S. Connor, "Review of jet reconstruction algorithms", Ryan Atkin J. Phys. Conf. Ser. 645 012008, 2015

[96] CMS Collaboration, "Jet energy scale and resolution in the CMS experiment in pp collisions at 8 TeV", JINST 12 (2017) P02014 [arXiv: 1607.03663]

[97] F. Beaudette, "The CMS Particle Flow Algorithm", 2014 [arXiv: 1401.8155]

[98] CMS Collaboration, "Identification of heavy-flavour jets with the CMS detector in pp collisions at 13 TeV", JINST 13 (2018) P05011 [arXiv: 1712.07158]

[99] CMS Collaboration, "Performance of missing transverse momentum reconstruction in proton-proton collisions at $\sqrt{s} = 13$ TeV using the CMS detector", JINST 14 (2019) P07004 [arXiv: 1903.06078

[100] L. Sonnenschein, "Analytical solution of ttbar dilepton equations", Phys.Rev.D73:054015, 2016

[101] M.H. Seymour and M. Marx, "Monte Carlo Event Generators", MCnet-13-05, 2013 [arXiv:1304.6677]

[102] B. Cabouat, J.R. Gaunt and K. Ostrolenk, "A Monte-Carlo Simulation of Double Parton Scattering", JHEP11(2019)061 [arXiv: 1906.04669]

[103] R. Placakyte, "Parton Distribution Functions", 2011 [arXiv:1111.5452]

[104] J. Alwall et all., "MadGraph 5 : Going Beyond", 2011 [arXiv:1106.0522]

[105] C. Oleari, "The POWHEG-BOX", Nucl.Phys.Proc.Suppl.205-206:36-41 [arXiv:1007.3893]

[106] S. Frixione et all., "The MC@NLO 4.0 Event Generator", CERN-TH/2010-216 [arXiv: 1010.0819]

[107] B. Webber, "Parton shower Monte Carlo event generators", Scholarpedia

[108] M. Bahr et all., "Herwig++ Physics and Manual", Eur.Phys.J.C58:639-707, 2008 [arXiv: 0803.0883]

[109] T. Sjostrand, "A Brief Introduction to PYTHIA 8.1" Comput.Phys.Commun.178:852-867, 2008 [arXiv: 0710.3820]

[110] A. Karneyeu et all., "MCPLOTS: a particle physics resource based on volunteer computing", European Physical Journal C 74 (2014) [arXiv: 1306.3436]

[111] V. Lefebure and S. Banerjee, "CMS Simulation Software Using Geant4", CMS-NOTE-1999-072, 1999

[112] S. Banerjee, "Validation of Geant4 Physics Models Using Collision Data from the LHC", J. Phys.: Conf. Ser. 898 042005

[113] A. Rizzi, G. Petrucciani and M. Peruzzi, "A further reduction in CMS event data for analysis: the NANOAOD format", J. Phys.: Conf. Ser. 214 06021

[114] C.G. Lester and D.J. Summers, "Measuring masses of semi-invisibly decaying particles pair produced at hadron colliders", Phys.Lett.B463:99-103, 1999

[115] K. Bloom, "CMS software and computing for LHC Run 2", ICHEP 2016 [arXiv: 1611.03215]

[116] W. Tanenbaum, "A ROOT/IO Based Software Framework for CMS", ECONFC0303241:TUKT010, 2003

[117] CMS Collaboration, "CMS Luminosity Measurements for the 2016 Data Taking Period", CMS-PAS-LUM-17-001, 2017

[118] CMS Collaboration, "CMS Luminosity Measurements for the 2017 Data Taking Period", CMS-PAS-LUM-17-001, 2018

[119] CMS Collaboration, "CMS Luminosity Measurements for the 2018 Data Taking Period", CMS-PAS-LUM-17-001, 2019

[120] CMS Twiki, "Baseline muon selections for Run-II", 2019

[121] CMS Collaboration, "BRIL Work Suite"